Springer Ser Chem Sens Biosens (2007) 5: 303–338
DOI 10.1007/5346_031

Published online: 29 July 2006

The Quartz Crystal Microbalance in Cell Biology: Basics and Applications

Vanessa Heitmann · Björn Reiß · Joachim Wegener (✉)

Institute for Biochemistry, Westfälische Wilhelms-University, Wilhelm-Klemm Str. 2, 48149 Münster, Germany
wegenej@uni-muenster.de

Abstract This chapter describes recent studies in which the quartz crystal microbalance (QCM) technology has been applied as a monitoring tool for animal cells in vitro. With shear wave resonators used as growth substrates it is possible to follow the de novo formation or the modulation of established cell–substrate contacts from readings of the resonance frequency with a time resolution in the order of seconds. From cell adhesion studies it became clear that different cell types induce an individual shift of the resonance frequency but it has been a matter of debate, which subcellular structures determine the individual impact of a given cell type on the QCM response. This question has been addressed by our group in recent years and a summary of our current understanding of this problem will be given here. Different approaches have been applied to challenge the cells in a well-defined way and to monitor the associated changes of the QCM readout. Taken together, these studies have led us to the following conclusions: (i) The cellular bodies primarily lead to an increased energy dissipation that does not correspond to a simple

viscous behavior. (ii) The adhesive proteins underneath the cells provide a measurable contribution to the overall QCM response of adherent cells. (iii) The average distance between lower cell membrane and substrate surface does not have a significant impact on the acoustic load situation. (iv) The QCM is sensitive to cell stiffness and reports in a similar way on changes in cell stiffness, as accessible from scanning force microscopy measurements. (v) The cortical actin cytoskeleton is a dominant contributor to the cells' acoustic response.

Keywords QCM · Cell–substrate interactions · Cell adhesion · Cell spreading · Extracellular matrix · Cellular micromechanics · Cytoskeleton · Cell elasticity · Liposomes · Impedance analysis

Abbreviations

QCM	Quartz crystal microbalance
ECIS	Electric cell–substrate impedance sensing
RICM	Reflection interference contrast microscopy
FLIC	Fluorescence interference contrast microscopy
HC	Hydrocortisone
SFM	Scanning force microscopy

1 QCM as an Emerging Tool in Cell Biology

The quartz crystal microbalance (QCM) was already well-known and established as an analytical tool for studying adsorption phenomena at the solid–liquid interface [1–4] when its potential for studying cell–substrate adhesion was recognized. As reviewed in preceding chapters of this book, the QCM approach is based on thin disks made from α-quartz that are sandwiched between two metal electrodes. Due to the piezoelectric nature of α-quartz, an oscillating electrical potential difference between the two surface electrodes induces a mechanical oscillation of the crystal and vice versa. For QCM purposes, only AT-cut resonators are used that perform shear oscillations parallel to the surface with the maximum amplitude at the crystal faces [5]. The resonance frequency of the mechanical oscillation responds very sensitively to the adsorption of any material upon the resonator surface. In 1959 a linear relationship between the observed shift in resonance frequency and the amount of mass deposited on the surface was established by Sauerbrey [6]. The so-called Sauerbrey equation is, however, only valid for rigid and homogeneous mass films that move synchronously with the resonator surface. If these conditions are met, the device is sensitive enough to report on mass depositions in the submicrogram regime. In a typical bioanalytical application, a receptor molecule (e.g., cell surface receptor, antibody) is immobilized on the quartz surface and the ligand is offered from solution, or the other way round [7, 8].

As soon as molecular recognition and binding occurs, a shift in the resonance frequency of the crystal is induced. The frequency shift can be easily measured and – as long as the Sauerbrey conditions are fulfilled – interpreted in terms of mass increase. It is the strength of the technique to provide label-free, mass-sensitive detection of the binding reaction at the crystal surface in real time.

It was then recognized that the adhesion of cells to the quartz surface also induced a shift in resonance frequency that was shown to be linearly correlated with the fractional surface coverage [9, 10]. Time-resolved measurements of the resonance frequency were then used to follow the attachment and spreading of cells to the quartz surface, with extraordinary time resolution. Comparison with established cytological techniques has proven that the QCM readout reports reliably on the number of cells on the surface and the time course of adhesion [9, 11, 12]. But the technique is more versatile. A few studies have been published in which the QCM is used as a transducer in cell-based drug testing assays [13–15]. Here the change in resonance frequency of already established cell layers serves as a very sensitive measure for changes in cell vitality, which are often mirrored in an perturbed substrate adhesion. Clearly, the technique is still in its infancy with respect to in vitro drug and toxicity testing. But, an enormous number of fundamental or applied scientific problems in cell biology may take advantage of the QCM approach in the future, in particular since the quartz resonators are easily integrated into any cell culture vessel and multi-well devices will be available soon.

However, in order to explore the full potential of the QCM device for cell biological applications it is imperative to understand the individual contributions of subcellular components to the overall signal in detail. A pool of experimental observations exists indicating that the QCM is primarily sensitive to mechanical phenomena associated with the ventral (i.e., the lower, substrate-facing) membrane and the molecular architecture of cell–substrate adhesion sites [16]. To the best of our knowledge, there is only one study in the literature that reports on resonance frequency shifts in response to cellular activities at the apical (upper) membrane. Here, Cans et al. [17] described measurements in which butting and retrieval of exocytotic vesicles was monitored, which only occurs at the site of the cell that is not facing the substrate. In all other reports the observed changes of the QCM parameters could be attributed to the cell–substrate adhesion zone plus the ventral, substrate-facing membrane. It is, however, unclear how parameters like the density of cell–substrate contact sites, the topography of the cell–substrate adhesion zone, or the mechanical properties of the cytoskeleton exert an individual impact on the QCM signal. When all subcellular contributions have been identified, the number of QCM applications in cell biology will increase and the full potential of the technique will be visible. Thus, the present chapter will focus on these questions and provide a few answers as they are known today.

2
Lessons from Cell Adhesion

Although cell adhesion studies based on QCM readings have been successfully performed for many years and are widely known, they will be addressed here in more detail in order to emphasize certain insights extracted from these simple-to-perform experiments. Figure 1 shows a schematic of the experimental setup that was used in our laboratory to measure the shift in resonance frequency during attachment and spreading [12].

The quartz resonator with a fundamental resonance frequency of 5 MHz forms the bottom plate of a measuring chamber that holds approximately 0.5 mL of cell suspension. The oscillation at minimum impedance is stabilized by a feedback-control oscillator circuit[1] that is placed close to the crystal inside a temperature-controlled Faraday cage (37 °C). The oscillator circuit is driven by a 5 V power supply and the resonance frequency is determined by a commercially available frequency counter.

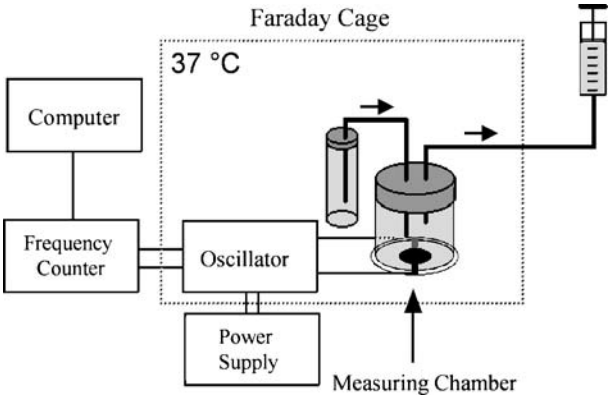

Fig. 1 Experimental setup to monitor the time course of cell attachment and detachment by reading the resonance frequency of the quartz resonator that forms the bottom plate of a cell culture vessel. The measuring chamber is housed in a 37 °C incubator. When an exchange of culture fluid is needed, for instance to expose the cells to some trigger compound, a corresponding reservoir is also placed inside the incubator with a simple transfer mechanism as indicated

2.1
Time Course of Attachment and Spreading

Cells were seeded into the measuring chamber in a sterile flow hood. Immediately afterwards attachment and spreading of the cells was followed with time. Figure 2a compares the time-dependent shift in resonance frequency when

[1] The oscillator circuit based on a Texas Instruments TTL chip was developed by A. Janshoff.

increasing amounts of epithelial MDCK II cells are seeded into the chamber at time zero.

From the upper to the lower part of Fig. 2a the cell density in the measuring chamber was continuously increased from a cell-free control to a maximum of 1.5×10^6 cells cm^{-2}. In the very early phase of all curves there is a moderate increase of the resonance frequency by 50 to 100 Hz, which is exclusively due to warming of the medium inside the chamber to 37 °C. After a transient maximum the resonance frequency continuously decreases and thereby mirrors the formation of cell–substrate adhesion sites and continuous progress in cell attachment and spreading. The time resolution of such measurements can be reduced well below one second so that even very subtle details of the cell adhesion kinetics are available using QCM measurements. The more cells are seeded, the bigger is the resulting shift in resonance frequency upon attachment and spreading.

When the maximum frequency shift Δf_{max} for an individual experiment, as shown in Fig. 2a, is plotted against the number of cells seeded into the measuring chamber at time zero, we obtained a saturation type relationship that is presented in Fig. 2b. We have interpreted this result as follows: as long

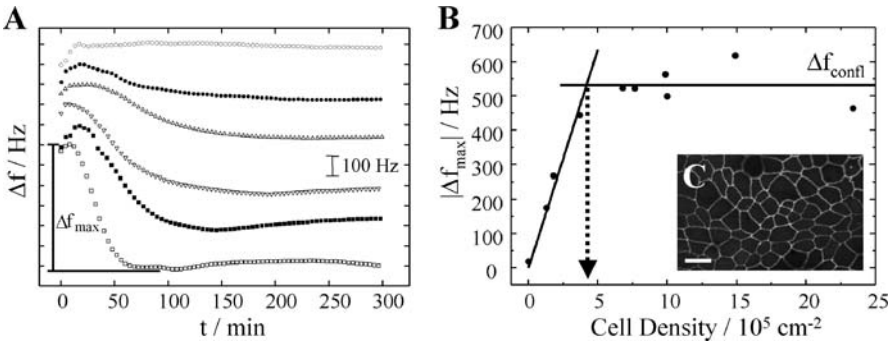

Fig. 2 **a** Shift of the resonance frequency during attachment and spreading of initially suspended MDCK II cells. Each curve represents a different number of cells that were seeded at time zero. From the *upper* to the *lower curve* seeding densities were as follows (in cm^{-2}): *open circles* 0; *filled circles* 1.3×10^5; *up triangle* 1.8×10^5; *down triangle* 3.7×10^5; *filled squares* 7.7×10^5; *open squares* 1.5×10^6. Δf_{max} indicates the maximum frequency shift observed for a given seeding density. Please note that an offset was used to present all experiments together in one figure. **b** Maximum frequency shift Δf_{max} as a function of cell density seeded into the measuring chamber at time zero in the experiments shown in **a**. The data is analyzed by a two-case approach: (i) For low cell densities the *ascending line* indicates the linear correlation between surface coverage and frequency shift. (ii) For high seeding densities a *horizontal regression line* is applied that represents the frequency shift associated with a confluent cell layer. The intersection of lines (i) and (ii) corresponds to the number of cells on the surface (per unit area). **c** Fluorescence micrograph of a confluent MDCK II cell layer after staining for a junctional protein exclusively localized at the cell border. *Scale bar* represents 20 μm

as the density of seeded cells is small enough that all cells reaching the surface can find an adhesion site, an increase in the maximum resonance frequency shift $|\Delta f_{max}|$ is observed with increasing seeding density. This frequency shift is proportional to the fractional surface coverage. However, when the number of seeded cells is further increased, all adhesion sites are occupied and consistently we do not find any further increase in $|\Delta f_{max}|$. This observation already implies that the QCM device is primarily sensitive to phenomena that occur at the quartz surface but does not report on cells that are beyond the first cell monolayer. Based on this data it is hard to imagine that biological activities that occur at the apical surface of an established cell layer can be observed by QCM.

If this interpretation is valid, we should be able to determine the number of cells that actually adhered onto the quartz surface from measurements like those shown in Fig. 2b. To do so, we have chosen a two-case approach: (i) for low seeding densities the relationship is approximated by a straight line with positive slope that indicates the linear correlation between frequency shift and surface coverage; (ii) beyond a certain cell density the experimental adhesion curve is modeled by a horizontal line indicating that any surplus of cells, which do not find an adhesion site on the substrate, does not contribute to the measured QCM response. Accordingly, the interception between the two straight lines should mark the actual cell density on the surface. For the MDCK cells (strain II) that were used in these experiments, we found the interception to be located at a seeding density of $4.3 \pm 0.5 \times 10^5$ cells cm^{-2} (arrow in Fig. 2b). In order to validate this result we have also determined microscopically the cell density in an entirely confluent monolayer after the cell borders had been stained by immunocytochemistry. Figure 2c shows a typical fluorescence micrograph that was used to determine the cell density. Images recorded by fluorescence microscopy revealed a cell density of $5.5 \pm 0.3 \times 10^5$ cells cm^{-2} on the surface, which is slightly above the value extracted from QCM readings. However, microscopic experiments were conducted on cell monolayers that were allowed to grow to confluence for several days while QCM experiments were limited to attachment and spreading within 5 h. Since the cells tend to multiply to some degree even in a confluent monolayer, it is not surprising to find somewhat higher cell densities in our microscopic control experiments. Repeating these kind of experiments with other cell types confirmed our conclusions. We found consistently that the basic interpretation of the data is valid and that the number of cells on the surface is determined correctly from QCM readings.

Table 1 compares the QCM-based cell density on the surface for MDCK cells strain I (MDCK I), MDCK cells strain II (MDCK II) and 3T3 fibroblasts with the outcome of cell density estimates derived from microscopic images [12]. The final shifts in resonance frequency that we observed when the resonator was completely covered by a continuous cell monolayer of either kind (Δf_{confl}) are also summarized in Table 1. Interestingly, different cell

Table 1 Shifts of the resonance frequency Δf_{confl} induced by attachment and spreading of different cell types. In all cases the resonator was completely covered with cells at the end of the experiment. The number of cells per unit area on the surface is determined from QCM experiments N_{QCM} and compared to a microscopic determination N_{Mic}

Cell type	Δf_{confl} (Hz)	N_{QCM} ($10^5 \times \text{cm}^{-2}$)	N_{Mic} ($10^5 \times \text{cm}^{-2}$)
MDCK II	530 ± 25	4.3 ± 0.5	5.5 ± 0.3
MDCK I	320 ± 20	3.1 ± 0.4	3.7 ± 0.2
3T3	240 ± 15	1.9 ± 0.5	1.3 ± 0.1
BAEC	40 ± 5	n.d.	n.d.

types create individual shifts in resonance frequency when they adhere to the quartz surface. It is important to stress that these differences are not due to incomplete coverage of the quartz resonator but mirror individual differences in the contact mechanics. Indeed, the key question is: *what are the factors that give rise to this individual frequency response and what cellular property is mirrored therein*?

2.2 Specific or Non-Specific Surface Interactions

Before addressing this topic it might be helpful to mention for readers unfamiliar with the subject, that cells do not interact directly with an in vitro surface but only with proteins or polysaccharides that are adsorbed to it. The cells express certain cell-surface receptors that are specialized to recognize and *specifically* bind to these adhesion-promoting proteins on the surface. The major class of these cell-surface receptors specialized on binding to extracellular adhesive proteins are the so-called *integrins*. Since both, the cell surface and the growth substrate are decorated with ionic or polar groups, there are also many *non-specific* electrostatic or electrodynamic interactions involved in cell adhesion. It has been a matter of long scientific debate and discussion whether specific or non-specific interactions are predominantly responsible for anchorage of cells to a given surface [18–20]. Nowadays it is widely accepted that both specific and non-specific interactions contribute, but there is compelling evidence that specific ligand–receptor interactions are more important for the final strength and the dynamic properties of the adhesion sites [18]. Thus, the question arises whether the QCM response requires specific, receptor-mediated adhesion of the cells to the surface or whether the sole presence of the cell body close to the resonator surface is sufficient to induce the observed QCM response.

To answer this question we tried to block the specific interactions between cell-surface receptors and adhesive proteins on the substrate by adding

short peptides to the culture fluid that correspond to the amino acid sequence within the primary structure of adhesive proteins that integrins bind to. When these soluble peptides are added to the cell suspension, they compete for the receptor binding site and delay or omit specific interactions with substrate-immobilized proteins.

In our experiments we used serum containing medium as culture fluid. Serum naturally contains the adhesive proteins vitronectin (VN) and fibronectin (FN). Since these proteins adsorb instantaneously from solution to the surface, there is no need to precoat the resonators with any other adhesive protein before. Both proteins, VN and FN, are recognized by cell surface receptors via the same amino acid sequence, namely Arg-Gly-Asp-Ser or RGDS in one letter code. Accordingly, we studied the impact of soluble peptides with this amino acid sequence on the time course of cell attachment and spreading as revealed by measurements of the resonance frequency. Figure 3 shows the outcome of four experiments in which either the penta-peptides Gly-Arg-Gly-Asp-Ser (GRGDS) and Ser-Asp-Gly-Arg-Gly (SDGRG), the tetra-peptide Arg-Gly-Asp-Ser (RGDS) or the tri-peptide Arg-Gly-Asp (RGD) are added to the cell suspension in a concentration of 1 mM each.

The two penta-peptides GRGDS and SDGRG contain exactly the same amino acids but in reverse order. Thereby, the two molecules carry the same charge density and would provide the same perturbation to non-specific interactions – if at all. However, due to the reversal of the amino acid sequence only GRGDS has the correct sequence to interact specifically with the integrins whereas SDGRG does not. The time course of the resonance frequency as presented in Fig. 3 clearly demonstrates that in the presence of 1 mM

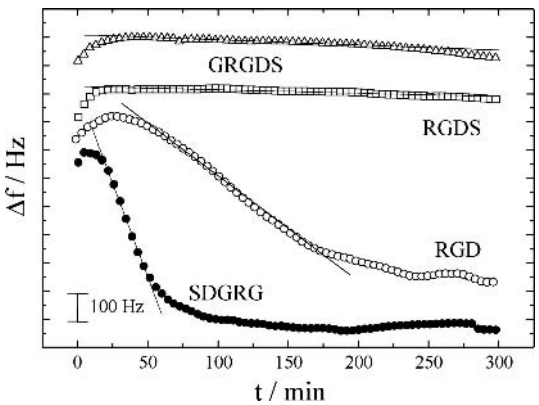

Fig. 3 Time course of attachment and spreading when equal amounts of MDCK II cells were seeded into the quartz dish in presence of the soluble peptides Arg-Gly-Asp (RGD), Arg-Gly-Asp-Ser (RGDS), Gly-Arg-Gly-Asp-Ser (GRGDS), and Ser-Asp-Gly-Arg-Gly (SDGRG). The concentration of each peptide was 1 mM, the cell densitiy was adjusted to 8×10^5 cm^{-2}

GRGDS the resonance frequency does not indicate any cell adhesion to the resonator surface. In contrast, when SDGRG is added to the culture fluid, there is no difference compared to experiments in which no peptide is present at all (compare Fig. 2a). Thus, when specific interactions between cell-surface receptors and substrate-immobilized proteins are not allowed to form, we do not observe any measurable impact on QCM readings. Apparently, loose attachment of the cell bodies to the substratum does not produce any significant acoustic load [12, 16].

When the amino acid sequence of the soluble peptides is gradually shortened by removing first the initial G from GRGDS giving RGDS (GRGDS → RGDS), followed by removal of the final S from RGDS yielding RGD (RGDS → RGD), the peptides eventually lose their potency to inhibit cell adhesion. While RGDS is still capable of blocking cell adhesion completely when applied in 1 mM concentrations, the same concentration of RGD is not (Fig. 3). These observations indicate that the final Ser is crucial in order to compete successfully for integrin binding sites. As shown in Fig. 3, the QCM readout provides the necessary sensitivity and time resolution to perform these kind of studies automatically.

For a correct interpretation of this data it is imperative to learn more about the situation at the crystal surface when specific interactions are blocked by RGDS-containing peptides. One technique that allows visualization of the "footprints" of cells on a surface is reflection interference contrast microscopy or short RICM. Practically, RICM is limited to transparent growth substrates so that we conducted a correlation experiment on ordinary coverslips instead of quartz resonators. In these experiments we seeded cells in serum-containing medium that was either supplemented with 1 mM RGDS or not. In both cases, the cells were allowed to attach and spread on the glass surface for 200 min before we recorded RICM images of each sample. Figure 4 provides a comparison of the recorded RICM images for both situations.

In Fig. 4a the cells form typical cell-surface junctions with the protein decorated growth substrate. The footprints indicate a spread morphology under these conditions. When RGDS is present in the medium the situation is rather different. As shown in Fig. 4b the cells are hardly visible in the RICM image although they have settled to the surface in this particular field of view. Bright field images taken from the very same spot (not shown) clearly prove that this is not a cell-free area of the substrate. In the center of the image (arrow) a typical fringe pattern reveals a small projection of a cell reaching to the surface. Based on the principles of RICM image formation and some technical parameters of the microscope, one can estimate that the lower cell membrane must be farther away from the substrate surface than 100 nm, probably significantly more. Apparently the presence of the cell bodies within this distance from the substrate surface and with only a very limited contact area – like a hard sphere on a flat surface – does not provide any significant acoustic load for the quartz resonator.

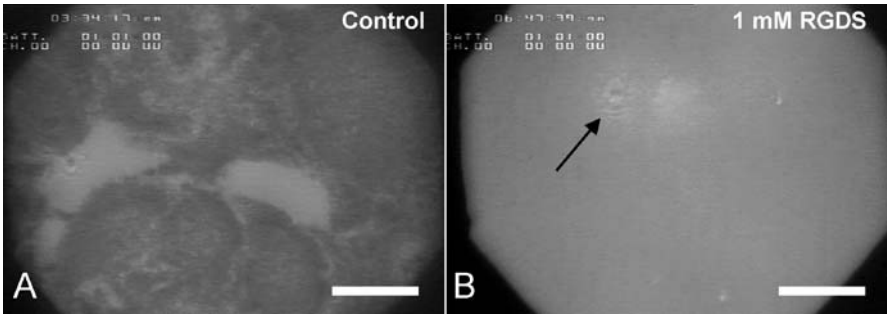

Fig. 4 RICM micrographs of MDCK II cells 200 min after seeding. The cells in **a** were suspended in serum-containing medium with no inhibitory peptides included, while the cells in **b** were exposed to 1 mM RGDS in the bathing fluid. The *black arrow* indicates the presence of a cell body that does not make close contact with the surface. *Scale bar* represents 10 μm

Thus, two main conclusions can be drawn from these experiments: (i) The QCM does only report on cells that are specifically anchored to the resonator surface. The method is blind to cells that just settle to the surface and attach only loosely. (ii) When specific cell–substrate interactions are omitted, the cells stay away from the surface by more than 100 nm, according to our RICM data. Theoretical considerations have previously indicated that cells may approach the surface as closely as 5–10 nm just by non-specific attraction [21]. This is, however, not confirmed by our optical measurements.

Looking more deeply at QCM principles, further support arises for the fact that the cells do not approach the surface as closely as 5–10 nm when specific interactions are blocked. According to Eq. 1 the penetration depth of the shear wave in an aqueous environment δ is approximately 250 nm at room temperature:

$$\delta = \sqrt{\frac{\eta_{\mathrm{fl}}}{\pi \cdot f \cdot \rho_{\mathrm{fl}}}}\,. \tag{1}$$

However, since the loosely attached cell bodies do not create any significant acoustic load on the resonator, they seem to be far enough from the quartz surface that the shear wave does not hit them with considerable amplitude. In one of the following chapters we will get back to these experiments and put them in context with further studies on confluent cell monolayers.

2.3 Titrating Cell–Substrate Contacts

Similar experiments as the ones shown in Fig. 3 have also been performed with different concentrations of RGDS-peptides. It was the objective of these

studies to *titrate* the cell–substrate adhesion sites and use the QCM response as an experimental indicator. We found that increasing concentrations of RGDS do not alter the final frequency response that is characteristically found for a given cell type, but the time course of the frequency shift is altered dramatically. Above a certain threshold concentration of RGDS the process of attachment and spreading was considerably delayed but in the long run we always observed a very similar final response, as in control experiments without any interfering peptides. Apparently the cell has certain mechanisms to overcome integrin blockade by RGDS with time. Several mechanisms could account for this observation: (i) When the integrin receptors are occupied by the peptide, they become internalized and fresh receptors are recruited to the cell surface. (ii) The cells synthesize and secrete their own extracellular matrix proteins at the site of cell adhesion so that the protein concentration and, thus, the number of binding sites on the surface continuously increases until RGDS blockade becomes ineffective. The observed behavior may also be a combination of both effects.

Even though RGDS blockade was not permanent it is possible to use QCM measurements to quantify the inhibitory effect of a given RGDS concentration from the slope of the curve during the first 5 h after inoculation. Figure 5 presents the results of such a series of measurements. The slope derived from the time course of the frequency shift is plotted as a function of RGDS concentration on a semilogarithmic scale. As anticipated, the curve is sigmoidal in nature and it is possible to derive the concentration of half maximum efficiency (EC_{50}) to $6 \pm 1\,\mu$M.

Following cell adhesion and spreading in the presence of soluble peptides that mimic the recognition sequence of adhesive proteins was historically the

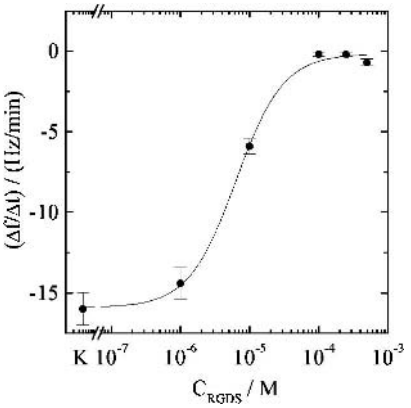

Fig. 5 Slope of the attachment curve of MDCK II cells as a function of RGDS concentration present in the bathing fluid. The concentration of half-maximum efficiency EC_{50} was determined to $6 \pm 1\,\mu$M RGDS

most direct experiment for learning about these binding sites and to identify them [22, 23]. At the time, the readout was based on time-lapse microscopy or colorimetric assays. In the future the QCM may serve as an alternative monitoring device in these kind of studies with outstanding sensitivity and the opportunity to automate the experiment for higher compound throughput in industrial screening.

Titration of cell adhesion sites may also be performed in the opposite direction when cell detachment is used as an experimental indicator. Then cells are first grown to confluence on the shear wave resonators and the competing peptides are then added to the bathing fluid. Once these peptides reach the site of cell–substrate adhesion they may displace the adhesive proteins from the receptor binding site and thereby loosen cell–substrate contacts. Figure 6 shows two examples for such experiments in which confluent Swiss 3T3 fibroblasts were exposed to 1 mM SDGRG or GRGDS (see above). Besides very minor changes, which are due to fluid handling, SDGRG does not induce any significant changes of the resonance frequency (Fig. 6a). Thus, the cell–substrate adhesion is not affected, consistent with the inverse amino acid sequence of this peptide. However, when GRGDS is added to the established 3T3 cell layers, an immediate rise of the resonance frequency is observed that stabilizes after 200 min. The frequency shift amounts to more than 150 Hz, which indicates that the cell layer is entirely removed.

Similar results were obtained when the cells were detached from the surface by means of EDTA, which chelates all divalent cations, that are necessary for stable cell adhesion (not shown).

What can be learnt from these kind of experiments with respect to the superordinate question, *what determines the QCM response of a given cell type*?

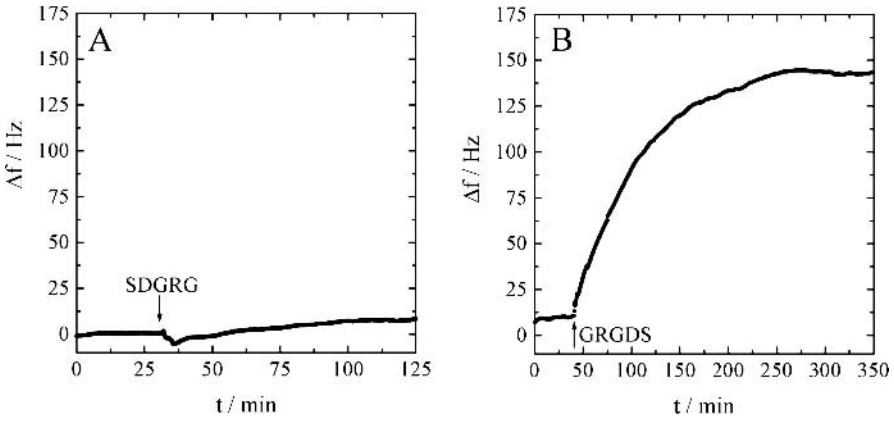

Fig. 6 Time course of the resonance frequency when preestablished, confluent monolayers of 3T3 fibroblasts were exposed to the penta-peptides SDGRG (**a**) or GRGDS (**b**) in 1 mM concentration, respectively. Addition of the peptides is indicated by *black arrows*

Unfortunately the answer is, *not very much*. These studies do indeed show that the QCM approach is a very sensitive tool for studying any perturbation of cell–substrate interactions in real time and with a highly quantitative readout. But the system itself is too complicated and holds too many variables to draw significant conclusions on the number of binding sites between cell and surface just from measurements of attachment and spreading in the presence of specific inhibitors. The enormous complexity arises from phenomena like: (i) When one integrin–protein interaction is blocked, another one of a different kind may take over the dominant role and mediate cell adhesion. This is easily possible since many integrins are promiscuous with respect to the proteins they bind to. (ii) Different cell types may express individual mixtures of integrins with graded affinities to the ECM proteins. Thus, a comparative study among different cell types is difficult to interpret. It seems that the only way to learn more about the underlying principles of the QCM response to adherent cells is using well-defined model systems with a significantly reduced complexity.

2.4 Cell Adhesion Versus Liposome Adsorption

In order to understand the laws that determine the QCM response towards the anchorage of living cells, it seemed helpful to use chemically well-defined model systems [24–26] that allow more systematic studies. By using liposomes with varying amounts of biotinylated lipids we tried to mimic the cell body (liposome) and its cell surface receptors (biotin moieties). The adhesive proteins on the surface were modeled by a layer of predeposited avidin that provides binding sites for the biotin residues in the lipid shell. Thus, receptor density and protein concentration on the surface have been under experimental control and can be adapted according to the experimental needs. In our initial studies we used large unilamellar vesicles made from dipalmitoylphosphatidylcholine (DPPC) doped with increasing molar ratios of dipalmitoylphosphatidylethanolamine (DPPE) that carried a biotin residue. The biotin was covalently attached to the lipid headgroup via a C_6 spacer.

In these experiments we used a technical setup that was originally described by Rodahl and coworkers [27] and is referred to as QCM-D. This device not only records the change in resonance frequency Δf but also changes of the so-called dissipation factor D, which is the inverse of the quality factor Q of the oscillation:

$$D = \frac{1}{Q} = \frac{Dissipated\ energy\ per\ cycle}{Stored\ energy\ per\ cycle} \tag{2}$$

According to Eq. 2 the shift ΔD mirrors changes in energy dissipation of the shear oscillation. Measuring the change in energy dissipation becomes im-

portant whenever systems are studied that do not behave like a rigid mass. Only for homogeneous mass films can an experimentally observed frequency shift be attributed unequivocally to mass deposition to the resonator surface according to the Sauerbrey relationship [6]. When the microviscosity or elasticity close to the quartz surface changes, the Sauerbrey equation no longer holds since these effects change the resonance frequency as well and are indistinguishable from simple mass deposition. Thus, viscous energy losses can make QCM measurements ambiguous and hard to interpret, if at all [28]. The device developed by Rodahl and coworkers overcomes this problem by recording both the shift in resonance frequency and the energy dissipation at a time which makes data interpretation more robust and provides twice the information of the system under study.

When living cells are studied within this setup we typically found frequency shifts Δf between 50 and 500 Hz, dependent on the cell type. The cell-type specific change in dissipation factor ΔD ranged between 1 and 4×10^{-4}. When we used undoped DPPC liposomes of 100 nm diameter that were allowed to settle on an avidin-coated resonator, we recorded frequency shifts in the order of 400–500 Hz, thus very similar to the readout for living cells. However, with respect to energy dissipation the liposomes behaved completely different. For the undoped DPPC liposomes we only observed an increase in energy dissipation in the order of 3×10^{-5}, which is roughly an order of magnitude less than that recorded for the substrate-anchored cells. Adding biotin-labeled lipids into the liposome shell, in order to allow for molecular recognition between liposome and surface bound protein, led to a gradual reduction of both Δf and ΔD. As demonstrated in Fig. 7 there is a gradual drop in both parameters with increasing concentrations of biotin residues in the liposome shell. In other words, the more ligand–receptor pairs were available the more the QCM response was reduced [24].

The reason for this unexpected behavior was revealed by scanning force microscopy [29]. With increasing biotin loaded into the liposome shell, the liposomes spread out on the surface. Eventually, they rupture when the adhesion forces provided by the ligand–receptor interactions dominate over the intermolecular forces between individual lipids in the liposome shell. The ruptured liposomes eventually form a lipid double-layer on the surface with the water-filled interior of the original liposome being emptied into the bulk phase. These lipid bilayers on the surface behave essentially like a rigid mass deposited on the surface so that the shifts in resonance frequency and dissipation decline.

So in a sense, these experiments suggest that liposomes, as they were used here, are not a suitable model system for systematic studies on cell-surface interactions by QCM, mostly due to the unavoidable rupture of the liposome when surface attraction becomes too strong. Nevertheless, for intermediate biotin concentrations these experiments did provide important information since they indicate that an aqueous compartment surrounded

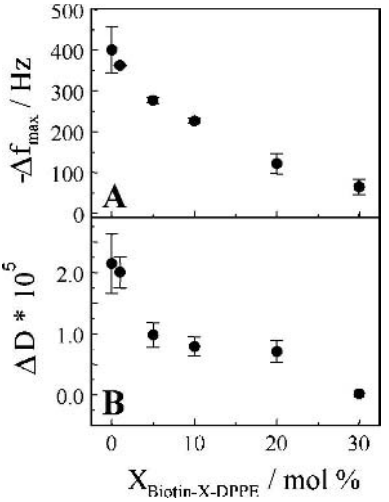

Fig. 7 Summary of liposome adhesion studies as performed with a QCM-D setup described in the text. *Panel A* shows the frequency shift Δf when the concentration of biotinylated lipids in the liposome shell is gradually increased. *Panel B* summarizes shifts of the dissipation factor ΔD from the same experiments. Data points are averages of at least two independent experiments

by a lipid double-layer is not sufficient to explain the acoustic load that is exerted on the resonator by a confluent cell layer. There is more to it than just a membrane-confined fluid compartment close to the surface. And this result is not dependent on the size of the liposome. The data in Fig. 7 was recorded for large unilamellar liposomes with an average diameter of 100 nm, but giant liposomes with diameters in the micrometer range show a similar behavior. Even for these vesicles, which have roughly the size of a typical animal cell, we could not observe an energy dissipation similar to that observed for adherent cells[2]. In a later paragraph we will address this issue again and demonstrate experimentally that the cortical cytoskeleton underlying the plasma membrane of living cells is very important for understanding their acoustic behavior in QCM experiments.

3 Analyzing Confluent Cell Layers

In the preceding sections we have studied the time course of cell attachment and spreading upon the resonator surface, dependent on the cell number and the presence of anti-adhesive peptides. The following paragraphs will

[2] Information provided by A. Janshoff.

describe experiments that were performed with confluent cell monolayers that had been preestablished on the resonator surface prior to the QCM experiment. A variety of cell types was included in these experiments in order to find cell-type specific differences that can lead to a better understanding of the system. Instead of reading the resonance frequency of the free oscillation we applied impedance analysis in a frequency range close to the fundamental resonance of 5 MHz.

3.1 Impedance Analysis of the Shear Oscillation

The experimental setup to perform impedance analysis of the loaded resonator is shown in Fig. 8a.

The quartz disk is used as the bottom plate of a cell culture vessel and is mounted in a temperature controlled crystal holder (37 °C). The surface electrodes on either side of the quartz are connected to an impedance analyzer (Solatron Instruments, SI-1260) operating in continuous wave mode. The frequency-dependent complex impedance $Z(f)$ returned by the impedance analyzer is expressed as magnitude of impedance $|Z|(f)$ and phase shift between voltage and current $\Phi(f)$. The raw data is analyzed by the well-known Butterworth–Van Dyke (BVD) equivalent circuit with the lumped impedance elements C_0, R_q, L_q, C_q and Z_L. R_q, L_q and C_q represent the piezoelectric properties of the unperturbed resonator itself, whereas C_0 summarizes its dielectric properties and all parasitic contributions arising from contacts and wiring. The load material in contact with the resonator surface is represented by the complex impedance Z_L. As long as the resonator is not loaded too

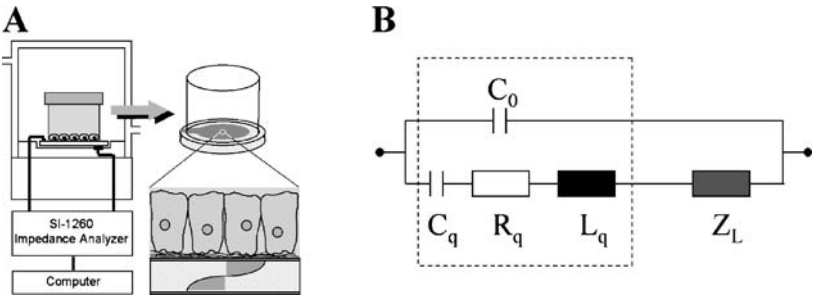

Fig. 8 **a** Experimental setup to perform impedance analysis of the shear oscillation. Quartz resonators are used as the bottom plate of a measuring chamber that is mounted in a temperature-controlled Faraday cage. Impedance data is recorded with a gain/phase analyzer in the vicinity of the fundamental resonance of 5 MHz (typically from 4.97 MHz to 5.04 MHz). **b** Butterworth–Van Dyke equivalent circuit to analyze the impedance raw data of the loaded resonator. All parameters except Z_L are assigned to the unperturbed resonator whereas Z_L denotes the impedance of the load material (cell layer) on the resonator surface

heavily, the BVD circuit is a good approximation for the more complex and comprehensive Mason model [30] that is well suited to describe any load situation [31]. For low-load conditions, for which the BVD approximation is valid, the electrical impedance of the material in contact to the resonator Z_L is directly proportional to its acoustic impedance $Z_{m,L}$ as given in Eq. 3:

$$Z_L = \frac{\pi}{4K^2\omega_0 C_0}\frac{Z_{m,L}}{Z_{m,q}}, \tag{3}$$

with the acoustic impedance of quartz $Z_{m,q}$, the electrochemical coupling constant K^2, and the angular resonance frequency ω_0. For the cellular systems studied here it is difficult, if not impossible, to confirm the validity of the low-load condition ($Z_{m,L} \ll Z_{m,q}$). However, recent studies have shown that even for heavy mass ($\leq 5\ \mathrm{mg\,cm^{-2}}$) or viscous loading ($\eta\rho \leq 1000\ \mathrm{g^2\,cm^{-4}\,s^{-1}}$), the lumped equivalent circuit is still in very good agreement with the distributed Mason model (deviations $\leq 1\%$) [32]. For simple and laterally homogeneous material films some of their mechanical properties can be deduced from the acoustic impedance, like for instance, their density or elasticity modulus G. For complex systems like layers of living cells, this is not possible yet. However, it is the objective of the experiments described in this chapter to increase our understanding of these systems and to pave the way for a more quantitative acoustic analysis.

Figure 9 compares the frequency spectra of the impedance modulus $|Z|$ and phase shift Φ for resonators with or without a confluent layer of cells on the surface. In either case, the measuring chamber is filled with cell culture medium so that the resonator is always at least under liquid loading.

The presence of the cells (compared to medium only) gives rise to a strong impact on both quantities, $Z(f)$ and $\Phi(f)$, and is most obviously expressed in a significant damping of the shear oscillation, or in other words an increase in energy dissipation. Anchorage of the cells to the resonator induces only a minor shift of the impedance and phase spectra towards lower frequencies which would otherwise indicate an increase in energy storage. Since the cell-free but medium-loaded resonator (open symbols in Fig. 9) was always the beginning or end of any QCM experiment, we have chosen this as the basis relative to which the change in load impedance ΔZ_L due to the presence of different cell types on the resonator is expressed. The QCM response to culture medium was always very stable and highly reproducible. Thus, it was not necessary to run additional impedance experiments of the cleaned and dried resonator as a reference.

Quantitative analysis of the impedance data recorded with and without cells provides the change in the complex load impedance ΔZ_L that is due to the presence of cells on the resonator surface relative to medium loading. Table 2 compares the magnitude of the load impedance $\Delta|Z_L|$ for seven different cell types that had been grown to confluence prior to the QCM experiment. The change in load impedance varies considerably for the var-

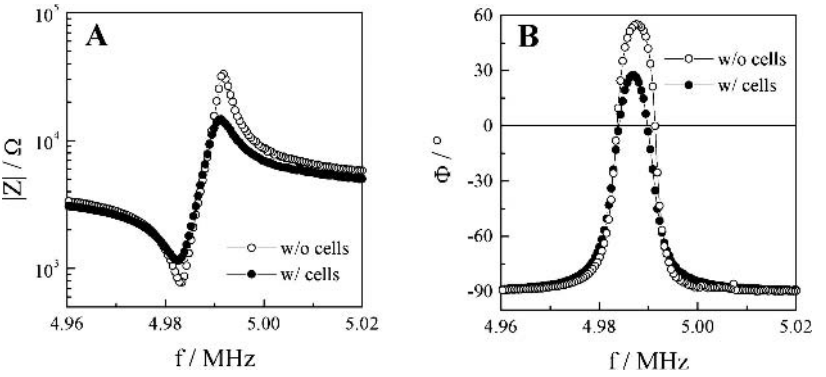

Fig. 9 Experimental raw data of the shear oscillation as recorded by impedance spectroscopy. **a** Impedance magnitude of a cell-covered and a cell-free resonator as a function of frequency. **b** Phase spectra of a cell-covered (*filled circles*) and a cell-free (*open circles*) resonator in comparison

Table 2 Change in the load impedance of quartz resonators covered with confluent layers of different cell types relative to resonators in contact with culture medium only. The complex load impedance ΔZ_L is expressed by its magnitude $\Delta|Z_L|$ as well as in its real and imaginary components

Cell type	$\Delta\|Z_{load}\|$ (Ω)	$\Delta\text{Real}(Z_{load})$ (Ω)	$\Delta\text{Imag}(Z_{load})$ (Ω)
NRK	720 ± 60	700 ± 60	170 ± 15
MDCK I	550 ± 35	550 ± 35	80 ± 22
MDCK II	425 ± 26	425 ± 26	19 ± 10
HUVEC	435 ± 65	405 ± 70	157 ± 16
PBCEC	380 ± 23	370 ± 25	79 ± 22
3T3	247 ± 40	245 ± 40	– 30 ± 30
BAEC	160 ± 13	99 ± 13	126 ± 14

ious cell types, very similar to the individual shifts in resonance frequency that were reported in the preceding sections (Table 1). The values range from 160 Ω for bovine aortic endothelial cells (BAEC) to a maximum of 725 Ω for epithelial-like normal rat kidney cells (NRK). Thus, the observed changes in load impedance $\Delta|Z_L|$ relative to a medium-loaded resonator differ by as much as a factor of five, dependent on the cell type. This reflects significantly different acoustic properties of the different cell types and probably also their individual anchorage to the resonator. Assigning these differences to a structural correlate is the problem to solve.

It is instructive to decompose the complex load impedance into its real (load resistance) and imaginary (load reactance) components. These two

quantities mirror the energy that is dissipated in the system – Real(Z_L) – or the energy that is elastically stored in the system – Imag(Z_L). Except for bovine aortic endothelial cells we have found that the dissipated energy is always many times larger than the stored energy. This was already apparent from the change in the spectra as discussed above. In this respect MDCK II cells represent the extreme, when the dissipated energy overcomes the stored energy by more than a factor of 20. For most other cell types this ratio is between two and ten. We only found for bovine aortic endothelial cells (BAEC) that the stored energy (imaginary) is bigger than the dissipated energy (real). However, these cells in general had only very little impact on the shear displacement so that it is somewhat questionable whether this deviation from the general trend observed for all other cells is real.

Taken together, these studies revealed that confluent cell layers in contact to the resonator lead to a significant increase of energy dissipation from the shear oscillation [33] as we had learned already from the QCM-D experiments presented in Sect. 2.4. The impact of the cells on energy dissipation is individual and dependent on the cell type. It is important to mention in this context that different batches of a certain cell line may also cause a different QCM response within certain limits. This is not surprising for cell biologists since cells of the same kind but taken from different batches may show a certain variance in their behavior and it underlines that the QCM is capable of picking up these subtle differences.

When we compare the acoustic behavior of the cells with simple and well-defined systems, the cells do not behave like a rigid and homogeneous mass layer. This is obvious from the occurrence of significant energy dissipation that cannot be found for rigid mass films. On the other hand, the cells also do not behave like a simple viscous (Newtonian) fluid such as water or water/glycerol mixtures. It has been shown many times in the past that Newtonian fluids increase the real and the imaginary part of the load impedance to the same degree, and the increase of both quantities scales linearly with the square-root of the density–viscosity product of the liquid [33, 34]. The reason for the increase of energy storage (reactance of the load impedance) observed for viscous fluids is assigned to (i) the synchronous movement of the first liquid layer that tightly adsorbs to the resonator surface (no slip behavior) and (ii) the entrainment of liquid in nano- or mesoscopic cavities on the surface due to surface roughness. These mechanisms do not apply to adherent cells, as can be concluded from the imaginary part of the load impedance that lags behind the real part [16].

This latter finding is indeed not surprising since the microscopic structure at the interface between an adherent cell and its growth substrate is very different from the wetting of viscous fluids upon the resonator surface. Figure 10 sketches the contact area between lower cell membrane and substrate surface, including the major structural components that contribute to cell adhesion. Most importantly, the cell membrane is not in direct contact with the

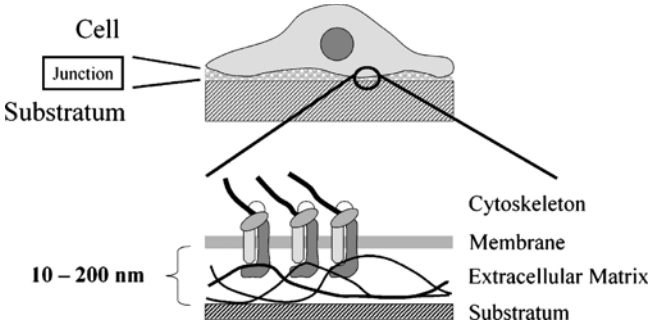

Fig. 10 Schematic of the interface between an adherent animal cell and a technical substratum. The blow-up provides a rough overview of the structural arrangement within the contact area in which cell membrane receptors bind to proteins immobilized on the substrate surface. It is important to note that there is a thin cleft between the lower cell membrane and the substratum that is approximately 10–200 nm in width

resonator surface but is hovering an average distance between 10 and 200 nm above, as mentioned in Sect. 2.2 already.

The thin cleft between substrate surface and plasma membrane is filled with an aqueous electrolyte solution that contains proteins, carbohydrates, and low molecular weight components. Anchorage to the surface is provided by cell-surface receptors that bind to adhesive proteins immobilized on the growth substrate. The most prominent cell surface receptors – the *integrins* – stick out of the membrane by approximately 20 nm and thereby bridge the gap between cell membrane and substratum. Very often these integrins are not evenly distributed in the plasma membrane but they tend to cluster to so-called *focal adhesions* or *focal contacts*. Focal contacts are adhesion sites in which the cells are believed to have the closest distance to the substrate. Thus, the interface between cell and substrate is not at all isotropic but is filled with filamentous polymers (proteins, sugars) and may have a gel-like constitution due to the water-storage capacities of the carbohydrates. Furthermore, the cell membrane may approach the surface closely in focal contacts (< 20 nm) but may be farther away in other areas underneath the same cell. So not only the molecular composition but also the width of the contact area is laterally heterogeneous.

3.2 No Correlation between Cell–Substrate Separation Distance and QCM Response

As mentioned in Sect. 2.2 the decay length of the shear wave into a viscous medium in contact wiht the resonator can be estimated from Eq. 1. If a 5 MHz resonator, as used in our studies, is loaded with pure water at room temperature, the characteristic axial decay length of the shear displacement amounts

to approximately 250 nm. When the fluid within the thin cleft underneath the cells is assumed to behave like water in a first approximation, then the decay length of the shear wave is in the same range as the average width of the cleft between cell membrane and growth substrate. Thus, the hypothesis arose that the individual QCM responses for different cell types may be due to the individual separation distances between cell body and resonator surface. As a consequence, the cells may have been exposed to different amplitudes of the propagating acoustic wave, which may in turn lead to an individual sensitivity of the QCM for these different cells.

In order to measure the average distance between lower cell membrane and growth substrate accurately, we made use of fluorescence interference contrast microscopy or FLIC, which has been recently developed by Lambacher, Braun, and Fromherz [35–37]. Readers interested in this novel technique and its theoretical background are referred to the above references as only a brief introduction will be given here. In FLIC, the cells are grown on silicon substrates that have regular steps of 5 μm $\times$ 5 μm made from silicon oxide on their surface. The step heights are well-defined and range between 20 and 200 nm and are, thus, only a fraction of the wavelength of visible light. After the cells have attached and cultured on these micropatterned FLIC substrates, their membranes are stained by a lipid-soluble fluorescent dye that integrates into the plasma membrane. When the cell-covered FLIC substrate is then placed in the incident light beam of a fluorescence microscope, the silicon/silicon oxide interface acts as a mirror and standing waves of the incident light are formed with a node at the silicon surface. Thus, the intensity of fluorochrome excitation is dependent on the distance between dye (membrane) and mirror (silicon). The same mechanism applies to the fluorescent light emitted by the fluorophore upon excitation so that the intensity of the fluorescent light is also modulated by the distance between dye (membrane) and mirror (silicon). Taken together, the intensity of the fluorescence light is a function of the cell–substrate separation distance and introduces a strong dependency of pixel brightness on distance between membrane and mirror. However, tracing fluorescence intensity versus distance between membrane and silicon substratum provides a (damped) periodic function so that any distance determination from a single fluorescence intensity reading is not unique. Introduction of terraces of silicon oxide of at least four different heights provides well-known spacers between cell membrane and reflecting interface such that four different fluorescent intensities are measured and analyzed. These four point measurement makes the intensity–distance relationship unique. Lambacher, Braun, and Fromherz developed an optical theory for this system with the distance between membrane and oxide surface as the only adjustable parameter [35, 37]. Fitting of this theory to the experimental data provides the cell-substrate separation distance. The accuracy of the FLIC approach has been estimated to be better than 1 nm.

We have performed FLIC microscopy for all cell types that have been listed in Table 2 in order to quantify their individual distance to the growth substrate. It is an inherent problem of this approach that the cells had to be grown on micropatterned silicon for FLIC measurements and not on a quartz resonator as used in QCM. But the uncertainty whether the cells behave differently on either substrate cannot be bypassed in principle. Figure 11 shows the change in load impedance $\Delta|Z_L|$ for the different cell types studied here as a function of their individual cell–substrate separation distance extracted from FLIC measurements. If the hypothesis applies that cells provide a more sustained QCM response the closer they are to the surface, one would have to expect a decrease of $\Delta|Z_L|$ with increasing distance d. The graph in Fig. 11, however, shows no obvious correlation between the acoustic load of the resonator and the distance between lower cell membrane and its surface. Please note that, for instance, BAEC and NRK cells show very similar distances from the surface of approximately 75 nm but the change in load impedance $\Delta|Z_L|$ differs by more than a factor of four.

Another very obvious deviation from the working hypothesis is given by the porcine brain capillary endothelial cells (PBCEC) that have been studied in the presence and absence of the steroid hormone hydrocortisone (±HC). As demonstrated in Fig. 11 the steroid does not change the distance between membrane and substrate surface significantly (101 ± 6 nm without HC versus 94 ± 3 nm with HC) but it does change the acoustic load of the resonator from $\Delta|Z_L| = 380\ \Omega$ (without HC) to $\Delta|Z_L| = 890\ \Omega$ (with HC) indicating that there is no direct correlation between both quantities.

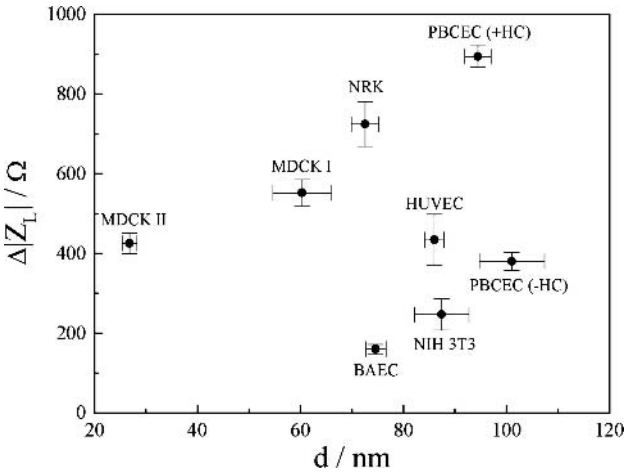

Fig. 11 Magnitude of the load impedance $\Delta|Z_L|$ for different cell types as a function of the individual distance d between their lower membrane and the substrate surface. The data does not show any correlation between both quantities, indicating that the distance between resonator and cell body is not dominating the QCM readout

Taken together, these studies show that cell–substrate separation distance is not the most significant parameter when explaining the acoustic load of shear wave resonators covered by confluent cell layers. It may still have a minor impact but the QCM response is apparently dominated by other mechanisms.

3.3
Adhesive Proteins Underneath the Cells Contribute to the QCM Readout

As sketched in Fig. 10 and mentioned before, the cells anchor to adhesive proteins that are immobilized on the surface. When cells are cultured for a certain time, they even produce their own adhesive proteins and secrete it into the space between membrane and substratum. Thus, we tried to address whether or not these adhesive proteins underneath the cell body may contribute to the total QCM readout of a confluent cell layer. Instead of limiting the analysis to preadsorbed layers of one or two purified proteins, we tried to study the complex extracellular material underneath the cells (extracellular matrix or ECM) by removing the cell bodies but leaving the macromolecular network of proteins and sugars behind on the substrate. The protocol required a combination of hypotonic stress and detergent extraction [16]. Microscopic inspection of reference substrates revealed that this procedure lifted the cell bodies effectively off the substrate. The surface was, however, still decorated with proteins as revealed by immunocytochemical staining.

Impedance analysis of the shear oscillation was performed for resonators covered with a confluent layer of cells and after the cell bodies had been removed by hypotonic lysis. The changes in load impedance ΔZ_L are again expressed relative to the identical quartz resonator that was loaded with protein-free medium only. Consistent with our expectation, we observed in these experiments that the magnitude of the load impedance $\Delta|Z_L|$ was significantly reduced when the cell bodies were removed from the resonator with only their ECM being left behind. In particular, the real component of ΔZ_L was barely detectable after cell removal and ranged in the order of 20–30 Ω for resonators that MDCK and 3T3 cells had been removed from. Please compare Table 2 for the corresponding values of the confluent cell layers, which ranged between 250 Ω for 3T3 and even 550 Ω for MDCK I. Accordingly, either the cell bodies themselves with their membranes and cytoskeleton or the liquid confined in the thin cleft underneath the cells must be the site of energy dissipation. As a matter of fact the complex protein and carbohydrate layer that remained on the surface does not show the considerable dissipating properties as one would expect. In a more recent study these results have been confirmed by Marx and coworkers [38].

It was, however, interesting to recognize that the load reactance, that mirrors the kinetically stored energy, was only reduced by 10 or 20% upon removal of the cell bodies with the ECM remaining on the surface. In some

rare cases we found a reduction of the load reactance by 50%, but never more than that. Although the acoustic properties of the extracellular matrix on the one hand and the cell bodies on the other are not strictly additive, it is reasonable to assume that a significant fraction of the load reactance observed for confluent cell monolayers, relative to a medium-loaded quartz, resides in the extracellular matrix that is adsorbed on the quartz surface [16]. This finding has to be recognized whenever the QCM response to an adherent cell monolayer is analyzed, interpreted, and modeled.

In general, all QCM measurements that were done with resonators initially coated with a confluent cell monolayer, which was later removed by hypotonic lysis, characteristically showed a load resistance at the limit of detection but a considerable load reactance. As discussed in the preceding section, this is a typical behavior of rigid mass films that adsorb to the resonator surface. Apparently the ECM remaining on the surface behaves like an adsorbed mass layer that does not provide any significant energy dissipation. The remaining load reactance disappeared when the surface was exposed to the protease *trypsin* indicating that the remaining material on the resonator was primarily made from protein.

A very similar result was found when we coated the resonator with a layer of collagen. In a typical experiment we measured an increase for $\Delta|Z_L|$ of $236 \pm 18\ \Omega$ relative to a medium-loaded resonator. Decomposing the complex load impedance in real and imaginary components revealed a load resistance of $43 \pm 15\ \Omega$ compared to a load reactance of $232 \pm 18\ \Omega$. Thus, the layer of purified collagen shows similar acoustic properties as the remaining ECM on the surface [16].

3.4
Cortical Actin–Cytoskeleton is a Major Contributor

The mechanical properties of living cells are significantly determined by the cytoskeleton. There are three major classes of protein filaments that belong to the cytoskeleton and have individual functions: microfilaments, intermediate filaments, and microtubules [39]. Whereas microfilaments and microtubules are highly dynamic structures that can form rapidly by polymerization of actin or tubulin monomers, respectively, the intermediate filaments are stationary structures that are important for the basal mechanical stability of the cell but not for dynamic changes. Since the microfilaments are composed of filamentous actin they are also referred to as actin filaments [39]. Both expressions can be used synonymous.

With respect to the mechanical properties of the plasma membrane the microfilament system is considered the most important since a network of these filaments underlies the plasma membrane and stabilizes it. This membrane supporting network of actin filaments is often called the *cortical actin*. In order to test whether the mechanical properties of the membrane (de-

termined to a large degree by the cortical cytoskeleton) contributes to the acoustic load on the resonator surface we applied different strategies to modulate the actin cytoskeleton. By adding a membrane-permeable drug that interferes with actin polymerization we were able to decompose actin filaments in the corresponding monomers. On the other hand, we cross-linked and stiffened all cellular protein by chemical fixatives and studied the associated QCM response.

3.4.1 Disintegration of Actin Filaments

Actin filaments are continuously assembled and disassembled in living cells by concomitant polymerization and depolymerization. Since the elongation and shortening of the filaments occur at opposing ends of the filaments, it is possible to distinguish between filament poles. The growing end is termed the *plus end* whereas the site of depolymerization is called the *minus end* [39]. The fungal toxin Cytochalasin D (CD) is a membrane-permeable compound of low molecular weight that specifically inhibits the polymerization of actin monomers into growing filaments but leaves depolymerization unaffected. Thus, when cells are exposed to this drug the actin filaments shorten and finally disappear [40]. Figure 12a and 12b provide microscopic images of

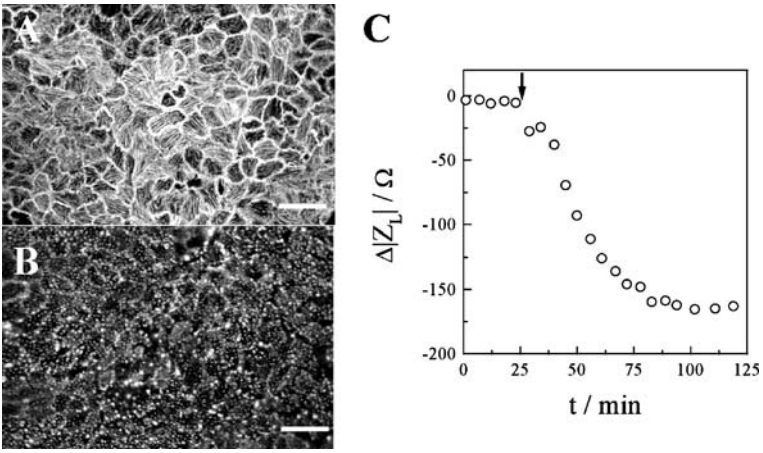

Fig. 12 Fluorescence micrographs of confluent MDCK II cell monolayers after the actin cytoskeleton has been stained by fluorescence-labeled phalloidin. **a** Control cells were not exposed to Cytochalasin D. **b** Cells were exposed to 5 μM Cytochalasin D for 100 min. The staining confirms that actin filaments have been degraded to small actin aggregates. The *scale bar* represents 25 μm. **c** Magnitude of the load impedance $\Delta|Z_L|$ as a function of time when confluent MDCK II cell monolayers were exposed to 5 μM Cytochalasin D at the time indicated by the *arrow*. The value of $|Z_L|$ at the beginning of the experiment was set to zero

confluent MDCK cells that have been stained for their actin cytoskeleton by fluorescence-labeled phalloidin, a compound that specifically binds to filamentous but not monomeric actin. The cells shown in Fig. 12a served as a control, whereas those in Fig. 12b were challenged with 5 μM CD for 100 min prior to fixation and staining.

In the control cells one can easily spot two very prominent actin structures: (i) *stress fibers* that run along the lower, substrate-facing membrane interconnecting two sites of cell–substrate adhesion and (ii) the *junctional actin ring* that follows the cell periphery and stabilizes cell-to-cell junctions. After exposure to CD both actin structures change dramatically. Instead of stress fibers and an actin belt around the cells, there are only actin aggregates that look like clumped monomeric actin without any filamentous structure. Thus, within 100 min of exposure time the actin filaments are disassembled. However, the cells remain spread and anchored to the growth substrate, so that after CD treatment there is still a confluent cell monolayer on the surface.

The same experiment was performed with MDCK cells that had been grown to confluence on quartz resonators. We then recorded impedance spectra under basal conditions, applied 5 μM CD and followed the acoustic load by continuously recording impedance data of the shear oscillation. In Fig. 12c the change in load impedance $\Delta|Z_L|$ is traced as a function of time in a typical experiment. Addition of CD is indicated by an arrow. Upon CD exposure the acoustic properties of the cell layer change considerably. Relative to the confluent MDCK II monolayer the magnitude of the load impedance $\Delta|Z_L|$ decreases by approximately 170 Ω, which is more than 40% of $\Delta|Z_L|$ for the intact cell layer. The time course in Fig. 12c correlates favorably with the time course of actin disassembly as monitored by microscopic studies similar to the ones shown in Fig. 12a,b. Decomposing Z_L into real and imaginary components reveals that both load resistance and load reactance contribute almost equally to the observed changes. In other words, we do see very similar changes in load resistance and load reactance under the influence of CD.

Treating cells with CD to disassemble their actin cytoskeleton has been described many times in the literature. When cells were studied by scanning force microscopy (SFM) after CD exposure, a significant reduction of membrane stiffness was reported for various cell types [41, 42]. Since the acoustic impedance also decreases, it seems reasonable to propose that the QCM may serve as a micromechanical probe to study membrane stiffness. Further experiments will be presented below that support this point of view.

In more general terms, the experiments described in this paragraph provide two major conclusions: (i) The actin cytoskeleton has a strong impact on the acoustic properties of the cell layer and (ii) the QCM is capable of monitoring functional changes in the cytoskeleton quantitatively and under physiological conditions. The second point should be emphasized since the

QCM provides this kind of readout without the necessity to open the incubator door. As the cells are anchored directly onto the surface of the mechanical transducer, the device can be easily integrated into biotechnological reactors or other experimental setups. Alternative techniques like scanning force microscopy or scanning acoustic microscopy [43] are more powerful in the sense that they may provide a laterally resolved elasticity mapping; however, due to the technical requirements of these devices, the cell cultures have to be manipulated and removed from their cell culture environment.

3.4.2 Cross-Linking all Cellular Protein by Chemical Fixatives

Motivated by the experimental findings that the QCM may serve as a micromechanical probe for monitoring membrane stiffness, we studied the QCM response when the cells on the resonator surface were treated with chemical fixatives that are known to cross-link all cellular proteins. Scanning force microscopy (elasticity mapping) has revealed that cross-linking of cell protein by aldehydes like glutaraldehyde (GA) or paraformaldehyde (PFA) stiffens the plasma membrane and increases the Young's modulus (a quantitative measure of mechanical stiffness) of the cells considerably [44, 45]. Thus, we monitored the acoustic response when confluent MDCK cell monolayers were exposed to either GA or PFA in concentrations that are typically used to prepare cytological samples. Upon exposure to 2.5% (v/v) glutaraldehyde for 30 min the load impedance relative to a medium-loaded resonator $\Delta|Z_L|$ increased from $472 \pm 72\,\Omega$ for the native MDCK II monolayer to $2340 \pm 245\,\Omega$ after fixation. Accordingly, protein cross-linking increased the load impedance more than fivefold. In a different set of experiments in which we applied 4% (w/v) paraformaldehyde instead of glutaraldehyde for 30 min we observed a change in load impedance $\Delta|Z_L|$ from $529 \pm 18\,\Omega$ for the native MDCK II cell layer to $1004 \pm 49\,\Omega$ after fixation. Here the relative increase of $\Delta|Z_L|$ is still twofold but less pronounced than in the case of GA.

The time course of protein cross-linking and the associated cell stiffening is rather fast with respect to the time resolution of the measurements. Figure 13 compares the time course of $\Delta|Z_L|$ for confluent MDCK II cells exposed to GA with a corresponding control that did not receive any fixative. For a meaningful, time-resolved monitoring of the cross-linking reaction by QCM measurements we had to dilute the GA solution tenfold to 0.25% (v/v) and still found that the system was stationary again after less than 10 min. The final increase of $\Delta|Z_L|$ was, however, the same as with the higher concentrations of GA. According to this data, the incubation time of 30 min, as chosen in the experiments described above, was more than sufficient to reach a steady state in the protein cross-linking reaction.

In order to correlate the acoustic response upon cell fixation with the change in Young's modulus of the same cells under identical conditions as in

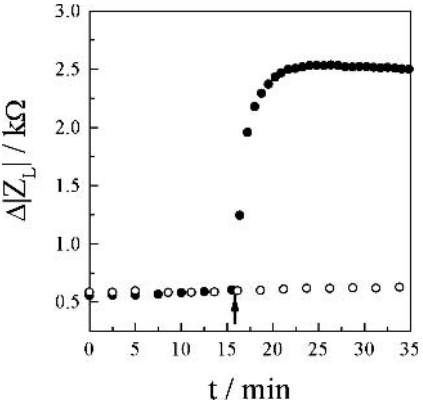

Fig. 13 Magnitude of the load impedance $\Delta|Z_L|$ relative to a medium-loaded resonator as a function of time when confluent MDCK II cell monolayers on the resonator surface are either treated with a 0.25% (v/v) solution of glutaraldehyde (*filled symbols*) or by a corresponding buffer control (*open symbols*). Addition of glutaraldehyde and buffer exchange are indicated by the *arrow*

QCM measurements, we also recorded elasticity maps of MDCK cells before and after fixation with PFA and GA by scanning force microscopy (SFM). Applying the commonly used Hertz model to the recorded raw data, we obtained a median Young's modulus of 2.5 ± 0.3 kPa for native MDCK cells that was increased to 3.7 ± 0.9 kPa after PFA fixation. The highest median values of 25 ± 3 kPa were found after a 30 min fixation with GA. Thus, the well-established SFM measurements indicate that there is a graded and individual stiffening of the cells when different fixatives are used. Consistent with the QCM experiments, PFA was found to be less efficient in cell stiffening than GA. In SFM studies the cortical actin cytoskeleton is considered to be the dominant contributor to the mechanical properties of the cell membrane [46]. Since the QCM readout correlates with SFM measurements, the conclusion may apply that the cortical actin cytoskeleton is also predominantly responsible for the acoustic load of the resonator.

We consider these studies to be strong evidence that the protein content of the cell, and in particular the cytoskeleton, is a prominent if not the predominant contributor to the acoustic load that is created on shear wave resonators by adherent cells. The reduction of $\Delta|Z_L|$ after disassembly of the actin cytoskeleton supports this hypothesis. Please note that all the experiments described in this paragraph have been performed with MDCK II cells. In order to exclude that the observed increase in acoustic load after fixation is a cell-type-specific phenomenon of MDCK II cells, analog experiments were performed with other cell types and returned the same answer. Only the numerical value of the increase in $\Delta|Z_L|$ varied to some extend.

3.4.3
Monitoring Steroid-Induced Changes in Cell Stiffness

In the preceding Sects. 3.4.1 and 3.4.2 we have described the QCM response to a disintegration of the actin cytoskeleton on the one hand and to cross-linking of all cellular protein by chemical fixatives on the other. The data implied that cell stiffness brought about by the cytoskeleton determines the acoustic response. However, the experimental means to arrive at this conclusion were rather drastic, in particular when chemical fixatives were applied. With respect to future applications of the QCM in cell biology it seems important to understand whether the technique is sensitive enough to monitor physiological alterations in cell stiffness. We therefore tested the QCM approach on an established phenomenon that has been published recently.

When endothelial cells isolated from porcine brain capillaries are grown in vitro, they respond in a very distinct way to the glucocorticoid hydrocortisone (HC) [47]. Upon exposure to this steroid in physiological concentrations, the cells have been shown to stiffen and improve their differentiation. The stiffening of the cells has been quantified by scanning force microscopy similar to the data presented above. The Young's modulus for these cells increases within 24 h from 5.1 ± 1.9 kPa to 8.3 ± 2.6 kPa when the medium is supplemented by 550 nM HC [48]. Apparently the stiffness of the cells increases due to the biochemical alterations induced by HC. The authors assign the observed stiffening of the cells to changes in the cortical actin network, since (i) the cortical actin is generally considered to be the decisive structure that determines cell stiffness and (ii) many studies have shown in various cell types that glucocorticoids like hydrocortisone may have an impact on cytoskeletal structures by regulating the expression of actin linker or actin bundling proteins [49].

When these cerebral endothelial cells are grown to confluence on quartz resonators under identical conditions as applied in the SFM studies, we observed an increase of the load impedance $\Delta|Z_L|$ from $380 \pm 23\,\Omega$ without HC to $890 \pm 27\,\Omega$ when the cells were treated with 550 nM hydrocortisone. Accordingly, the load impedance more than doubles in response to HC. Thus, QCM readings provide a similar answer to SFM with respect to the micromechanical changes that are induced in the cells by incubation with the hormone hydrocortisone. The QCM approach is obviously sensitive enough to monitor even physiological alterations within the cytoskeleton, which paves the way for many applications as a transducer for micromechanical changes in adherent cells.

Comparing QCM with the most established technique to study micromechanical changes in the plasma membrane of living cells, scanning force microscopy, there are advantages and limitations. Clearly, the QCM does not provide a laterally resolved image of the micromechanics within an adherent cell layer or even within different regions of a single cell. And at this point,

QCM readings cannot be translated into mechanical parameters that allow direct mechanical interpretation and modeling. On the other hand shear wave resonators provide (i) a much better time resolution than SFM, (ii) a readout that is averaged over many thousands of cells, and (iii) an entirely non-invasive measurement that can be easily automated and integrated into any cell culture vessel. Thus, the QCM may become an alternative or an additional means to study mechanical changes in adherent cells. It is important to recognize that SFM provides primarily the mechanical properties of the upper (apical) cell membrane whereas the QCM response is more sensitive to changes occurring in the lower (basal) cell membrane, so that SFM and QCM may complement each other.

4 Electrochemical QCM: New Options and New Insights

When the QCM is used as a mass-sensitive device in electrochemical experiments, it is often important to control the electrical potential of the electrode that is facing the liquid. Thus, an additional (reference) electrode is introduced into the QCM chamber in order to provide well-defined electrochemical conditions and to allow for various kinds of electrochemical reactions at the crystal surface. A well-known example is the electrodeposition of metals on the electrode surface that is often used to calibrate the device and calculate its mass sensitivity. When these kind of electrochemical studies are combined with QCM readings, the acronym EQCM is used, abbreviating electrochemical quartz crystal microbalance.

In order to extend the analytical options of the QCM measurement in cell biology we have introduced an additional low-impedance dipping electrode into the QCM chamber (compare Fig. 14) that serves as a counter electrode to perform electrochemical impedance analysis of the cells grown on the upper gold electrode of the quartz resonator.

Impedance analysis of cell-covered gold film electrodes in the frequency range between 1 Hz and 1 MHz was established more than 20 years ago as a non-invasive means to follow morphological changes in adherent cells [50–53]. The technique is referred to as electric cell–substrate impedance sensing or ECIS. The principle of ECIS relies on the fact that the cell bodies behave similarly to insulating particles at most frequencies that force the current to flow around the cell bodies. Accordingly, the overall impedance of the system increases when cells attach and spread on the electrode surface since the current has to pass through the narrow cleft between lower cell membrane and electrode surface before it can escape through the intercellular shunt between adjacent cells into the bathing fluid. Thus, the observed impedance increase originates from the cell–substrate adhesion zone as well as from the intercellular cleft that is often narrowed by cell-to-cell junctions [54]. Thus, ECIS

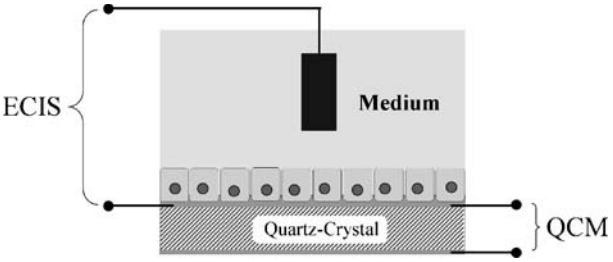

Fig. 14 Schematic of the combined QCM-ECIS setup. In order to perform electrochemical impedance analysis of the adherent cell layer on the substrate electrode, an additional low impedance platinum dipping electrode is introduced into the measurement chamber. Impedance analysis of the cell layer (ECIS mode) is performed in the frequency range between 1 Hz and 1 MHz, whereas the shear oscillation is analyzed close to its fundamental resonance between 4.97 MHz and 5.04 MHz. A computer-controlled relay allows switching between both modes automatically

readings can be used to follow both changes in cell–cell contacts as well as changes in the contact area to the conducting electrode surface. By selecting the AC sampling frequency properly, it is possible to make cell–cell or cell–substrate contacts dominate the overall impedance readout and thereby tune in on a certain portion of the cell bodies.

We have used this combined QCM-ECIS setup to study barrier-forming endothelial or epithelial cell layers that express tight intercellular contacts to occlude the paracellular shunt between adjacent cells. In vivo these cells serve as an interfacial cell layer that separates two fluid compartments and strictly regulates the exchange of solutes between both spaces. Examples are the lining of the blood vessels or the urinary bladder. In our experiments we used the epithelial cell line MDCK that originates from the lining of the kidney tubules and is a widespread model for a barrier forming cell layer. The QCM chamber was inoculated with a sufficiently high number of suspended MDCK II cells so that the growth substrate is completely covered after attachment and spreading without any need for further cell division. We then followed the establishment of a cell monolayer by continuously recording impedance data of the shear oscillation (*QCM mode*) on the one hand, and impedance data of the cells on the surface (*ECIS mode*) on the other hand. Switching between both modes was performed by a computer-controlled relay. Figure 15 compares the time course of the load impedance $\Delta|Z_L|$ as recorded in QCM mode as well as the time course of the electrode impedance (ECIS mode) at a sampling frequency of 400 Hz. The former reports on attachment and spreading of the cells whereas the latter indicates the formation of barrier-forming cell–cell contacts.

The time course of $\Delta|Z_L|$ is characterized by an immediate rise shortly after seeding the cells. After roughly 300 min the values stabilize before they

increase again to their maximum roughly 500 min after cell inoculation. The first part of the curve ($t < 300$ min) mirrors the kinetics of attachment and spreading of the cells in good accordance with microscopic studies and the resonance frequency measurements reported in Sect. 2.1. The second rise of $\Delta|Z_L|$ starting at $\sim 600\,\Omega$ till $\sim 800\,\Omega$ can, however, not be explained by a change in surface coverage. The additional load impedance must arise from acoustic changes within the cell bodies anchored to the quartz surface.

Triggered by our understanding of the contribution of the actin cytoskeleton, we stained for filamentous actin 3 and 10 h after cell inoculation. Microscopic images representative for the entire cell population are shown in Fig. 15. Approximately 3 h after seeding (Eq. 1) the cells are attached and fully spread but the actin cytoskeleton is not yet fully established. Diffuse actin is present but neither the very prominent actin belt around the cell periphery at cell–cell contact sites nor any stress fibers running along the lower cell membrane can be seen. The situation is different after 10 h of observation (Eq. 2). Staining of the actin filaments now reveals a continuous actin belt around the cells and stress fibers interconnecting individual focal adhesion sites. It seems plausible that shaping up of the actin cytoskeleton, as indicated by visible structural changes, induces the observed increase in load impedance and is thus detectable by QCM readings. Together with the experiments presented in Sect. 3.4 we take this observation as another experimental finding that supports our understanding that the actin cytoskeleton is an important contributor to the acoustic load of the resonator.

Figure 15 also shows the time course of the electrochemical impedance at a sampling frequency of 400 Hz (ECIS-mode). It is important to note that this dataset was recorded in exactly the same experiment and from the identical cell population that was used to collect the QCM data. Since both time traces originate from the same sample it is fair to compare the time course of both quantities in detail. The expression of barrier-forming cell–cell contacts cannot start before the cells have completely attached and spread on the electrode surface ($t > 300$ min). After 300 min the impedance starts to rise and is stationary again 700 min after cell inoculation, indicating full establishment of cell–cell contacts. The half-maximum barrier formation mirrored in the time course of the impedance at 400 Hz (ECIS) and the maximum of the load impedance $\Delta|Z_L|$ (QCM), which has been associated with the formation of a mature and polarized actin cytoskeleton, coincide at approximately 500 min. This finding strongly supports our understanding of the biphasic time course of the load impedance since it is well known from molecular cell biology that two adjacent cells have to form mechanically stable *adherens junctions* before they can establish barrier-forming *tight junctions* that occlude the intercellular shunt [54]. Adherens junctions are characterized by the thick actin belt that follows the cell periphery close to the apical pole. This actin belt can be easily spotted in Fig. 15 10 h after seeding but not 3 h after seeding.

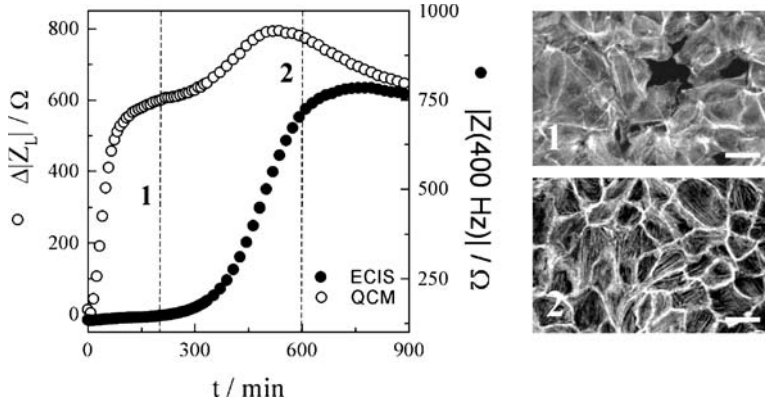

Fig. 15 Attachment, spreading, and differentiation of MDCK II cells followed by the combined QCM-ECIS approach. The change in load impedance $\Delta|Z_L|$ (*open circles*) reports on attachment, spreading, and reorganization of the actin cytoskeleton. The electrical impedance at 400 Hz (*filled symbols*) mirrors the establishment of barrier-forming cell-cell contacts and, thus, differentiation. The fluorescence micrographs in the *right panel* visualize the status of the actin cytoskeleton 3 h and 10 h after cell seeding. These time points are indicated in the graph by the *dashed lines* marked as *1* and *2*

Taken together, the combined QCM-ECIS approach provides the experimental options to follow attachment, spreading, cytoskeletal reorientation and cellular differentiation for barrier-forming cell types in a single experimental setup. Since the data is recorded from one and the same cell monolayer, the individual time courses of either parameter provide additional clues for a correct interpretation of the data. The electrochemical ECIS approach provides a lot more experimental options that have not been addressed in this article. These will help to broaden our understanding of QCM readings for adherent animal cells and guide us in the development of additional cell-based assays in which the QCM is used as a transducer to monitor cell behavior.

5
Outlook on QCM Applications in Cell Biology

The most obvious application of the QCM technology in biomedical research with living cells is the online observation of cell–substrate contacts, either when they form de novo as in attachment and spreading, or when established cell–substrate contacts reorganize under the influence of biological, chemical, or physical stimuli. It is a unique advantage of the QCM technique that these kinds of measurements are still possible when the quartz resonator is first coated with a thin layer of any technical material of interest like, for instance,

a metal or polymer film. Thus, the device may become an extremely useful tool for evaluating the cytocompatibility of technical surfaces, as required for the development of implants and other devices that need to be in contact with living tissue. The only limitation with respect to the pre-adsorbed material film on the resonator surface is that it is rigid in nature, of limited thickness and does not produce significant acoustic losses.

Even in more fundamental biomedical research the QCM is very versatile and broadly applicable. Proteins derived from native extracellular matrices may be deposited on the surface in order to study the interaction of cells with these protein coatings. A recent study by Li and coworkers [11] has shown that the QCM provides similar readouts as the traditionally applied cytological techniques. Due to its enormous time resolution even subtle differences in the kinetics of attachment and spreading become accessible.

Another striking new direction of the QCM in the field of cell biology are motility measurements based on noise analysis of the resonance frequency. When the cells move and crawl on the surface of the quartz plate the resonance frequency fluctuates as a direct consequence of the continuous assembly and disassembly of cell–substrate contacts during cell movement. Pax and coworkers have recently shown that the contraction of heart muscle cells can be easily recorded from the associated alterations of the resonance parameters [55]. We recently found that even in stationary cell layers without any open spaces that would allow for lateral migration, metabolically driven micromotion can be recorded [56].

All these different QCM modes can be used to develop whole-cell biosensors in which the cells serve as the sensory elements and the QCM device is used as a transducer. Of course the presence of living cells on the resonator surface provides certain practical limitations since the rather stringent experimental conditions required by living cells have to be met at all times. On the other hand, living cells allow monitoring the biological activity of the test compound rather than just the binding or blocking of some receptor binding site. Furthermore the assay may take advantage of intracellular amplification cascades, for instance second messenger cascades that provide a significantly improved sensitivity of the device.

Finally, the QCM can not only be used in a sensory mode but also as an actuator. It has been recently shown by Dultsev and coworkers [57] that virus particles deposited on the resonator surface may be displaced by increasing the shear amplitude of the resonator. Thus, it seems plausible that the resistance of cell–substrate interactions to lateral shear forces may be inferred from QCM measurements when the shear amplitude is increased to invasive magnitudes. The ease of the measurement, which can be automated and multiplexed, the rather simple experimental design, as well as the unique experimental access to the interface between living cells and technical substrates is very likely to create growing interest within the cell culture community for these new experimental options.

Acknowledgements The authors would like to express their gratitude to the Kurt-Eberhard-Bode Stiftung (Germany) for financial funding. VH is supported by the international Graduate School of Chemistry Muenster (GSC-MS, Germany). The expert help of Sandra Grunewald in preparing and maintaining the cell cultures is gratefully acknowledged.

References

1. Martin SJ, Granstaff VE, Frye GC (1991) Anal Chem 63:2272
2. Martin SJ, Frye GC, Ricco AJ (1993) Anal Chem 65:2910
3. Buttry D, Ward MD (1992) Chem Rev 92:1355
4. Bottom VE (1982) van Nostrand Reinhold Company, New York
5. Martin A, Hager HE (1989) J Appl Phys 65:2630
6. Sauerbrey G (1959) Z Phys 155:206
7. Janshoff A, Steinem C, Sieber M, el Baya A, Schmidt MA, Galla HJ (1997) Eur Biophys J 26:261
8. Janshoff A, Steinem C, Sieber M, Galla H-J (1996) Eur Biophys J 25:93
9. Gryte DM, Ward MD, Hu WS (1993) Biotechnol Prog 9:105
10. Redepenning J, Schlesinger TK, Mechalke EJ, Puleo DA, Bizios R (1993) Anal Chem 65:3378
11. Li J, Thielemann C, Reuning U, Johannsmann D (2005) Biosens Bioelectron 20:1333
12. Wegener J, Janshoff A, Galla HJ (1999) Eur Biophys J 28:26
13. Zhou T, Marx KA, Warren M, Schulze H, Braunhut SJ (2000) Biotechnol Prog 16:268
14. Marx KA, Zhou T, Montrone A, Schulze H, Braunhut SJ (2001) Biosens Bioelectron 16:773
15. Hug TS (2003) Assay Drug Dev Technol 1:479
16. Wegener J, Seebach J, Janshoff A, Galla HJ (2000) Biophys J 78:2821
17. Cans AS, Hook F, Shupliakov O, Ewing AG, Eriksson PS, Brodin L, Orwar O (2001) Anal Chem 73:5805
18. Bongrand P (1998) J Dispersion Sci Technol 19:963
19. Bell GI, Dembo M, Bongrand P (1984) Biophys J 45:1051
20. Pierres A, Benoliel AM, Bongrand P (2002) Eur Cells Mat 3:31
21. Vogler EA, Bussian (1987) J Biomed Mat Res 21:1197
22. Pierschbacher MD, Ruoslahti E (1987) J Biol Chem 262:17294
23. Pierschbacher MD, Ruoslahti E (1984) Nature 309:30
24. Reiss B, Janshoff A, Steinem C, Seebach J, Wegener J (2003) Langmuir 19:1816
25. Pignataro B, Steinem C, Galla HJ, Fuchs H, Janshoff A (2000) Biophys J 78:487
26. Luthgens E, Herrig A, Kastl K, Steinem C, Reiss B, Wegener J, Pignataro B, Janshoff A (2003) Meas Sci Technol 14:1865
27. Rodahl M, Höök F, Krozer A, Brzezinski P, Kasemo B (1995) Rev Sci Instrum 66:3924
28. Voinova MV, Jonson M, Kasemo B (2002) Biosens Bioelectron 17:835
29. Pignataro B, Steinem C, Galla HJ, Fuchs H, Janshoff A (2000) Biophys J 78:487
30. Rosenbaum JF (1988) Acoustic wave theory and devices. Artech House, Boston
31. Bandey HL, Martin SJ, Cernosek RW, Hillman AR (1999) Anal Chem 71:2205
32. Bandey HL, Hillman AR, Brown MJ, Martin SJ (1997) Faraday Discuss 107:105
33. Janshoff A, Wegener J, Sieber M, Galla HJ (1996) Eur Biophys J 25:93
34. Kanazawa KK, Gordon JG (1985) Anal Chem 57:1770
35. Lambacher A, Fromherz P (1996) Appl Phys A 63:207
36. Braun D, Fromherz P (1998) Phys Rev Lett 81:5241

37. Braun D, Fromherz P (1997) Appl Phys A 65:341
38. Marx KA, Zhou T, Montrone A, McIntosh D, Braunhut SJ (2005) Anal Biochem 343:23
39. Insall R, Machesky L (2001) Encyclopedia of life sciences. Wiley, Chichester
40. Brenner SL, Korn ED (1979) J Biol Chem 254:9982
41. Rotsch C, Braet F, Wisse E, Radmacher M (1997) Cell Biol Int 21:685
42. Hofmann UG, Rotsch C, Parak WJ, Radmacher M (1997) J Struct Biol 119:84
43. Bereiter-Hahn J, Karl I, Luers H, Voth M (1995) Biochem Cell Biol 73: 337
44. Shroff SG, Saner DR, Lal R (1995) Am J Physiol 269:C286
45. Hutter JL, Chen J, Wan WK, Uniyal S, Leabu M, Chan BM (2005) J Microsc 219:61
46. Rotsch C, Jacobson K, Radmacher M (1999) Proc Natl Acad Sci USA 96:921
47. Hoheisel D, Nitz T, Franke H, Wegener J, Hakvoort A, Tilling T, Galla HJ (1998) Biochem Biophys Res Commun 244:312
48. Schrot S, Weidenfeller C, Schaffer TE, Robenek H, Galla HJ (2005) Biophys J 89:3904
49. Castellino F, Heuser J, Marchetti S, Bruno B, Luini A (1992) Proc Natl Acad Sci USA 89:3775
50. Giaever I, Keese CR (1993) Nature 366:591
51. Giaever I, Keese CR (1991) Proc Natl Acad Sci USA 88:7896
52. Wegener J, Hakvoort A, Galla HJ (2000) Brain Res 853:115
53. Wegener J, Keese C, Giaever I (2002) Biotechniques 33:348
54. Wegener J (2003) Encyclopedia of life sciences. Wiley, Chichester
55. Pax M, Rieger J, Eibl RH, Thielemann C, Johannsmann D (2005) Analyst 130:1474
56. Sapper A, Wegener J, Janshoff A (2006) Anal Chem 78:5184
57. Dultsev FN, Ostanin VP, Klenerman D (2000) Langmuir 16:5036